Acta Materialia 106 (2016) 333–343

Contents lists available at ScienceDirect

Acta Materialia

journal homepage: www.elsevier.com/locate/actamat

Full length article

High-temperature functional behavior of single crystal $Ni_{51.2}Ti_{23.4}Hf_{25.4}$ shape memory alloy

L. Patriarca [a], H. Sehitoglu [a, *], E. Yu. Panchenko [b], Y.I. Chumlyakov [b]

[a] Department of Mechanical Science and Engineering, University of Illinois at Urbana-Champaign, 1206 W. Green St., Urbana, IL 61801, USA
[b] Siberian Physical-Technical Institute of Tomsk State University, Tomsk 634050, Russia

ARTICLE INFO

Article history:
Received 2 May 2015
Received in revised form
21 September 2015
Accepted 7 January 2016
Available online 26 January 2016

Keywords:
Shape memory alloy
Single crystals
Transformation strain
Digital image correlation
X-ray diffraction

ABSTRACT

In this work the functional behavior of the new $Ni_{51.2}Ti_{23.4}Hf_{25.4}$ high temperature shape memory alloy is investigated along three crystal orientations in compression and compared with the polycrystal behavior. Transformation temperatures were measured following specific aging treatments with the aim to optimize the shape memory and pseudoelastic behaviors. Two aging treatments were then selected in order to fulfill the optimum pseudoelastic behavior (500°C/4 h), and the maximum transformation temperatures (550°C/10 h) without compromising the alloy functionality. High temperature X-ray diffraction was utilized to determine the crystal orientations in the austenite phase for the single crystal specimens. The martensite structure was found to be the B19 orthorhombic, in contrast with monoclinic structure for lower Hf contents. Digital image correlation was successively used during isobaric strain-temperature experiments on the single crystal and polycrystal specimens. Large strain heterogeneities were found for the single crystals which pair with X-ray diffraction data that show un-transformed austenite below the martensite finish temperature. This reveals the heterogeneity of the austenite–to–martensite transformation for the present NiTiHf alloy which explains the divergence between the theoretical and experimental transformation strains. In addition, using digital image correlation it is possible to capture the local strain fields associated with fully transformed specimen regions. The transformation strains calculated locally are in close agreement with the theoretical transformation strains calculated with lattice deformation theory for the cubic austenite to the orthorhombic martensite phase transformation.

1. Introduction

NiTi-based shape memory alloys have become one of the most promising multi-functional materials since the addition of a ternary element enables to increase the transformation temperatures (TTs) above 100 °C, the strength and the stability of the binary NiTi alloy. Among several potential ternary elements (Hf, Zr, Pd, Pt and Au), the addition of Hf guarantees high TTs (>200 °C) with lower prices compared to the other alloying elements [1,2]. In the last years, a growing number of works have been published on NiTiHf alloys mainly focused on the effect of the composition, precipitation strengthening, mechanical and functional characterization of the polycrystal and texturized materials [3–5]. A comprehensive knowledge of the basic mechanical behavior has been achieved for Hf additions up to 20 at %, while less interest has been devoted to higher Hf compositions (>25 at %). Few works have been published on Hf alloying >25 at % (herein called Hf-rich NiTiHf alloys) on physical metallurgy [2,6–8]. In particular, no works have been published on the single crystal behavior. Since the potential high temperature applications of Hf-rich NiTiHf alloys, we investigate the mechanical and functional behaviors of the new $Ni_{51.2}Ti_{23.4}Hf_{25.4}$ composition along three different crystallographic orientations: [0 1 1], [1 1 1] and [3 4 14] with the aim to provide deeper insight into the mechanical behavior of Hf-rich NiTiHf alloys.

NiTiHf alloys are nowadays one of the most studied shape memory alloys (SMAs). The shifting of the transformations temperatures to >200 °C allows extending the usage of SMAs for many industrial applications (actuation, vibration damping, etc.). The possibility to use NiTiHf alloys as shape memory and pseudoelastic materials is accomplished by a proper selection of the composition and the successive heat treatments or, alternatively, specific

* Corresponding author.
E-mail address: huseyin@illinois.edu (H. Sehitoglu).

http://dx.doi.org/10.1016/j.actamat.2016.01.015
1359-6454/

processes. The selection of the composition is the major concern and there is still the need to investigate the optimum balance between the Ni and Hf contents depending on the specific requirements. Several works show that the martensite peak temperature (M_{PT}) remains constant for Ni-lean (<50 at %) $Ni_xTi_{90-x}Hf_{10}$ alloys at around 100 °C [1], while Hf additions lower than 10 at % do not lead to important changes in TTs [1,2,9]. The disadvantages of Ni-lean NiTiHf alloys are the poor mechanical properties in terms of ductility, cyclic stability and pseudoelasticity [5]. In order to overcome these drawbacks, the material community focused the attention to Ni-rich (>50 at %) NiTiHf alloys. Nevertheless the TTs display an abrupt decrease with Ni content between (50–51) at. %, the addition of the ternary element (Hf), followed by a proper aging treatment or process, provides benefits to the TTs and the mechanical properties. Depending on the desired material performances, Ni content can be increased up to 51 at % in order to optimize the shape memory and pseudoelastic behaviors. Besides, Hf content can be varied between (10–30) at. % based on the desired operational temperatures. Two of the most successful studied NiTiHf compositions are the $Ni_{50.3}Ti_{29.7}Hf_{20}$ [10–16] and the $Ni_{50.6}Ti_{29.4}Hf_{20}$ [17–20] which show perfect pseudoelasticity at temperatures near 250 °C. In the present work the new $Ni_{51.2}Ti_{23.4}Hf_{25.4}$ composition was selected in order to have good shape memory and pseudoelastic properties given by the high Ni content (Ni = 51.2 at %), along with high operational temperatures near 300 °C given by the high hafnium content (Hf = 25.4 at %).

Since NiTiHf alloys are still on relatively early stages of development, most of the research has been focused on the polycrystalline form of the material. Previous experimental and theoretical studies on NiTi single crystals [21–23], and more recent works on NiTiHfPd [24–26] and NiTiHf [15,27,28] single crystals have shown that the orientation strongly influences the maximum transformation strains of NiTi-based alloys. This derives from the selective activation of martensite variants upon loading along a specific transformation shear direction and habit plane. The transformation strain is also influenced by the crystal structures of the transforming phases. For NiTiHf alloys with Hf < 20 at % the phase transformation is accomplished by the transformation from the cubic B2 lattice to the monoclinic B19′ martensite phase. For this phase transformation different works have been published in the last decade covering both the experimental characterization and the theoretical calculations [11,13,28–37]. For the $Ni_{50.3}Ti_{29.7}Hf_{20}$ alloy, Stebner and co. calculated the transformation strains in compression to be approx. 8.5% for $[011]_{B2}$ and 6% for the $[111]_{B2}$ crystal orientations [27]. Less clear is the large difference between the measured strains (<3%) and the theoretical values. Another observation is that the phase transformation for Hf-rich NiTiHf alloys is considered to occur from the cubic B2 lattice to the orthorhombic B19 lattice [4]. In this work, evidence of the orthorhombic lattice for the martensite phase is provided using X-ray diffraction. This result enables to provide the correct basis for the theoretical calculations of the transformations strains. Understanding the austenite B2 to martensite B19 phase transformations is of fundamental importance in order to optimize the Hf-rich NiTiHf alloys for future high temperature applications.

Based on the choice of the NiTiHf composition, a proper aging treatment (temperature and time) fulfills its shape memory and pseudoelastic behaviors [3–5,9–12,16,18–20,27,33,38–40]. Aging affects the mechanical and functional behavior as the martensite morphology is strongly affected by the precipitate geometry (size and inter-particle distance), and by the precipitate coherency with the matrix [41,42]. Adopting the proper aging treatment, the precipitates formed during aging strengthen the matrix and provide thermal stability. Moreover, precipitation changes the basic chemical composition of the matrix. Yang and co [43]. provided the structural characterization of the H-phase formed in Ni-high NiTiHf alloys with Hf content ranging between (15–20) at. % following precipitation hardening. Successively, it was experimentally shown that this H-phase is slightly richer in Ni compared to the matrix with the consequence that the TTs are increased due to the depletion of Ni from the matrix [20,39]. Considering the importance of precipitation, we also provide a comprehensive study of the effects of the aging treatments on the TTs.

Isobaric and isothermal experiments were conducted using strain measurements obtained via Digital Image Correlation (DIC) technique [44]. DIC strain measurements enable to capture the local transformation region in both shape memory and pseudoelastic experiments, providing a straightforward measurement of the transformation strains [45–47]. Both the isothermal and isobaric experiments were conducted measuring the real time local strain fields on small surface areas of the specimens (typically 4 mm × 3 mm with a resolution of 2μm/px). The main advantage of this technique is that the strain data are not averaged over a large specimen length as, for example, with an extensometer. DIC strain measurements enable to capture the regions where the heterogeneous nucleation and growth of the martensite develops, neglecting the regions of the specimen where the transformation in not active. Such strain measurements are thus fundamental in providing a straightforward comparison with the theoretical calculations which assume the ideal transformation of the entire crystal from austenite to martensite.

In summary, in this work we present the mechanical and functional characterization of the new $Ni_{51.2}Ti_{23.4}Hf_{25.4}$ alloy focusing on three crystal orientations in compression: [0 1 1], [1 1 1] and [3 4 14]. Differential scanning calorimetry (DSC) was used to characterize the change of TTs with aging time and temperature. After proper selection of the heat treatments, isobaric and isothermal experiments were conducted using in-situ and ex-situ high-resolution DIC strain fields. Based on the local strain measurements and the X-ray diffraction data we discuss the well-known discrepancy between theoretical transformation strains with experimentally observed ones for NiTiHf alloys. A comparison of the single crystal behavior is also made with polycrystal behavior. The work points to gain further insight into the new $Ni_{51.2}Ti_{23.4}Hf_{25.4}$ alloy promoting further research efforts for making Hf-rich NiTiHf alloys suitable for industrial applications.

2. Experimental techniques

Polycrystal specimens with a composition of $Ni_{51.2}Ti_{23.4}Hf_{25.4}$ at.% were manufactured using plasma arc melting. Successively, single crystals were grown using the Bridgman technique in a He atmosphere from the polycrystal ingots. Compression specimens were sectioned into 3.8 mm × 3.8 mm × 8 mm using electro-discharged machining with the loading axis along the [0 1 1]$_{B2}$, [3 4 14]$_{B2}$, and [1 1 1]$_{B2}$ crystallographic directions. The specimens were successively homogenized at 1050 °C for 20 h under vacuum and successively slowly cooled inside the furnace to room temperature. The specimens were then solution-treated at 900 °C for 1 h in air followed by water quench. The chemical composition was checked by means of an ICP-MS PerkinElmer on two solution-treated polycrystal specimens to be Ni = 51.35%, Ti = 23.65% and Hf = 25.01%, and on two single crystal samples to be Ni = 51.25%, Ti = 23.35% and Hf = 25.4%. One of the single crystal compression specimens was successively sectioned into small samples with average weight of 60 mg suited for differential scanning calorimetry (DSC) technique. The samples were aged at temperatures ranging from 500 °C to 650 °C, and aging times between 2 h and 10 h. The samples were then polished using SiC paper in order to remove the thin oxide layer following solution-treatment and

aging. DSC was implemented by means of a Perking Elmer Pyris 1 differential scanning calorimeter with a heating/cooling rate of 60 °C/min. The heat flow data were recorded from room temperature to 450 °C. The heat flow data were used to determine the TTs variations following the specific heat treatments. More specifically, in the following we indicate the TTs using the Austenite peak temperature (A_{PT}) and the Martensite peak temperature (M_{PT}) obtained from the DSC curves.

Phase analysis and crystal orientation were determined by a Philips Xpert 2 X-ray diffractometer equipped with high temperature set-up. One 7 mm × 22 mm × 1.5 mm polycrystal specimen was sectioned by means of electro-discharged machining. The specimen was homogenized (1050°C/20 h in vacuum) and solution-treated (900°C/1 h followed by water quench). The crystal structure in austenite phase was determined at room temperature. Following the 600°C/4 h aging the same specimen was analyzed at room temperature for martensite structure characterization. The crystallographic orientations for the single crystal specimens were determined in austenite phase by means of X-ray diffraction conducted at 300 °C.

Isobaric and isothermal experiments were conducted using a MTS servo hydraulic load frame. Cooling of the compression grips was achieved with a customized copper coil surrounding the grips. Liquid nitrogen was used as the coolant in order to increment the cooling rate below 60 °C. A Lepel induction generator and a customized induction coil were used to heat the compression grips. The induction coil was properly designed in order to allow the temperature measurements using a Micro-epsilon infrared temperature sensor with a laser pointing the center of the compression specimens. The images suited for DIC strain measurements were captured on the opposite specimen surface by means of a IMI model IMB-202 FT CCD camera (1600 × 1200 pixels) with a Navitar optical lens. All the sides of the compression specimens were initially polished with SiC paper (P400) in order to remove any residual surface modification following EDM cutting and any residual oxides derived by the heat treatments. The specimen surface for DIC strain measurements was further polished with SiC paper up to P1500. The specimen surface selected for temperature measurements was covered with black paint. The speckle pattern for DIC strain measurements was deposited using black paint and an Iwata Micron B airbrush. Real time (*in-situ*) strain measurements were then obtained for a specimen region of approx. 3 mm × 4 mm with a resolution of 2.5μm/px. For both isobaric and isothermal experiments the specimens were initially heated up to 350 °C for 20 min in the fully austenitic region in order to stabilize the DIC speckle pattern at high temperatures. Once the speckle stabilization was reached, one image on the undeformed specimen (reference image) was captured. For isobaric experiments the reference image was captured at the maximum temperature and at zero load. The second (deformed) image was captured after applying the isobaric load at the same initial maximum temperature. Successive deformed images were captured every 5 °C from 350 °C to room temperature at constant load. For isothermal experiments the reference image was captured at zero load on the undeformed specimen. The images of the deformed specimens were captured every 2 s during isothermal loading and unloading.

3. Results

3.1. Transformation temperatures

The main DSC curves obtained in this work on the $Ni_{51.2}Ti_{23.4}Hf_{25.4}$ single crystal are reported in Fig. 1a. Following homogenization at 1050 °C for 20 h the slow cooling into the furnace produces the largest TTs measured for the $Ni_{51.2}Ti_{23.4}Hf_{25.4}$ alloy, $M_{PT} = 224$ °C and $A_{PT} = 285$ °C. Solution-treatment at 900 °C for 1 h shifts back the $A_{PT} = 104$ °C; the martensite peak for the solution-treated case was not detected. As shown in our previous publication [47], and in other works for similar NiTiHf compositions [13,16], aging temperatures below 500 °C are not investigated since the decrease of TTs after formation of ultra-fine precipitates rich of Hf. Several aging treatments (Fig. 1b) have shown to move the TTs in between the solution-treated and homogenized treatment TTs. Sixteen combinations of aging time and temperatures are reported in Fig. 1b. As a general guideline, increasing the aging temperature (from 500 °C to 650 °C) and the aging time (from 2 h to 10 h), leads to higher TTs. Further increments of the aging temperature (up to 700 °C) result in the saturation of the TTs, eventually in the decrease of the TTs for aging temperatures >700 °C being close to the solution-treatment temperature.

For the functional behavior of SMAs is also relevant to analyze the A_{PT}–M_{PT} peak–to–peak distance depending on the aging treatment. The minimum A_{PT}–M_{PT} is expected to optimize the

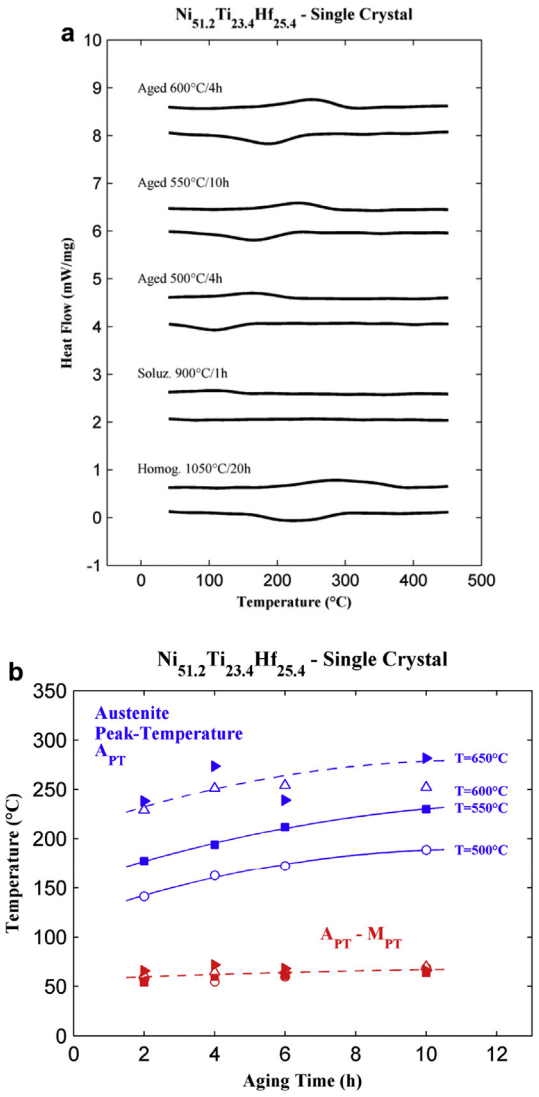

Fig. 1. (a) DSC curves for the most important heat treatments studied in this work. Homogenization produces the highest TTs, while solution-treatment shifts back the TTs as the precipitates formed during homogenization dissolve. Based on the adopted combination of aging temperature and time the TTs shift in between the homogenized and solution-treated cases. (b). Influence of the aging time and temperature on the austenite peak temperature (A_{PT}) and peak–to–peak (A_{PT}–M_{PT}) temperature.

functional behavior of shape memory alloys [48]. Fig. 1b shows that longer aging times slowly increase the A_{PT}–M_{PT} (approx. from 60 °C to 67 °C), and higher aging temperatures also increase the A_{PT}–M_{PT}, in particular for small aging times (at 4 h approx. from 55 °C to 72 °C). From all the aging treatments analyzed with DSC, we selected the most promising ones (see Fig. 1a): the 500°C/4 h minimizes the A_{PT}–M_{PT} = 55 °C, the 550°C/10 h leads to shape memory and pseudoelasticity at higher temperatures. Higher aging temperatures (600 °C and 650 °C) have not been considered since the detrimental effects on the pseudoelastic and shape memory behaviors generated by the precipitates formed at these temperatures. Fig. 1a shows that adopting 500°C/4 h and 550°C/10 h aging treatments, we mainly covered the potential TTs ranging from the solution-treated case to the homogenized. Moreover, we also study the effect of the aging time (4 h versus 10 h), other than the aging temperature (500 °C versus 550 °C). For the 500°C/4 h we measured the austenite start temperature as A_S = 109 °C, the austenite finish temperature as A_F = 225 °C, the martensite start temperature as M_S = 161 °C, and the martensite finish temperature as M_F = 39 °C. For the 550°C/10 h we measured A_S = 159 °C, A_F = 289 °C, M_S = 221 °C and M_F = 86 °C.

3.2. Material characterization

The X-ray diffraction pattern for the polycrystalline $Ni_{51.2}Ti_{23.4}Hf_{25.4}$ alloy is shown in Fig. 2. For the solution-treated condition (black line), the alloy is in fully B2 austenite state at room temperature. Peaks from B2 phase clearly appear following diffraction reflections from $(001)_{B2}$, $(011)_{B2}$, $(002)_{B2}$, and $(012)_{B2}$ planes. Following 600°C/4 h aging, two B2 peaks disappear, respectively the ones from $(011)_{B2}$ and $(012)_{B2}$ planes, while two new peaks appear which correspond to the diffraction reflections from the $(002)_{B19}$, and $(012)_{B19}$ planes of the orthorhombic B19 martensite phase. The peaks corresponding to the diffraction reflections of the B2 austenite from the $(001)_{B2}$ and $(002)_{B2}$ planes are still evident in the aged specimen even if the intensity of these two peaks is much lower than in the solution-treated case. This indicates that the austenite to martensite transformation is not fully completed. In Fig. 2 are also reported the atomistic structures utilized for indexing the diffraction patterns. The characteristics of the martensitic orthorhombic unit cell were obtained from Refs. [49], a = 3.02 Å, b = 4.20 Å and c = a = 4.69 Å. The structure of the austenite is the $L2_1$ composed by eight B2 unit cells with the experimentally calculated lattice constant a_0(B2) = 3.083 Å at RT.

3.3. Isobaric behavior

The summary of the isobaric experiments conducted on the three crystal orientations is reported in Fig. 3. Strains were calculated using DIC technique, a schematic of the strain measurements is reported in the top of Fig. 3. The strains reported refer to the axial strain component in the direction of the load. In the strain–temperature and stress–strain curves the black lines always refer to the axial strains averaged over the entire DIC region which is approximately 3.6 mm × 2.7 mm (bulk strain). The blue lines refer to the localized strains which are averaged over a smaller region (approximately 1 mm × 0.5 mm) where the largest localized strains develop (local strain). The images for correlation were captured every 5 °C, and the transformation strains were calculated as follows (schematic in the top of Fig. 3). Two lines were obtained with a

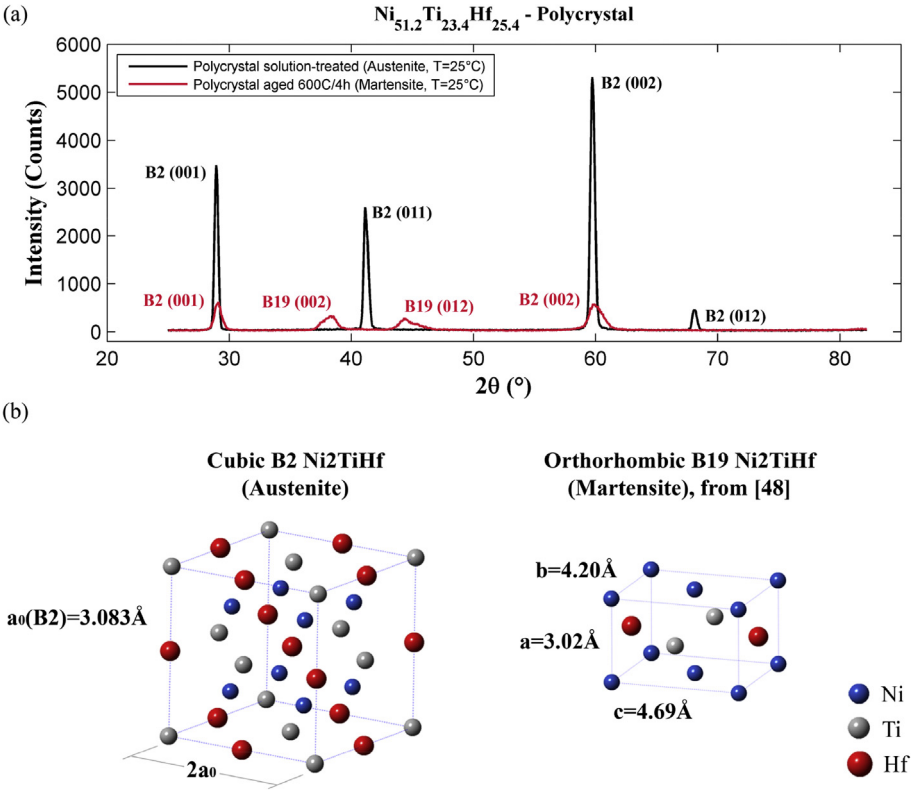

Fig. 2. (a) X-ray diffraction results showing the peaks from the austenite B2 structure for the polycrystal solution-treated specimen (black curve), and the peaks from the marteniste B19 structure for the polycrystal aged specimen (blue curve); (001) and (002) peaks of the un-transformed B2 austenite are still present in the aged condition; (b) crystal structures for the B2 austenite and for the orthorhombic B19 martensite. (For interpretation of the references to colour in this figure legend, the reader is referred to the web version of this article).

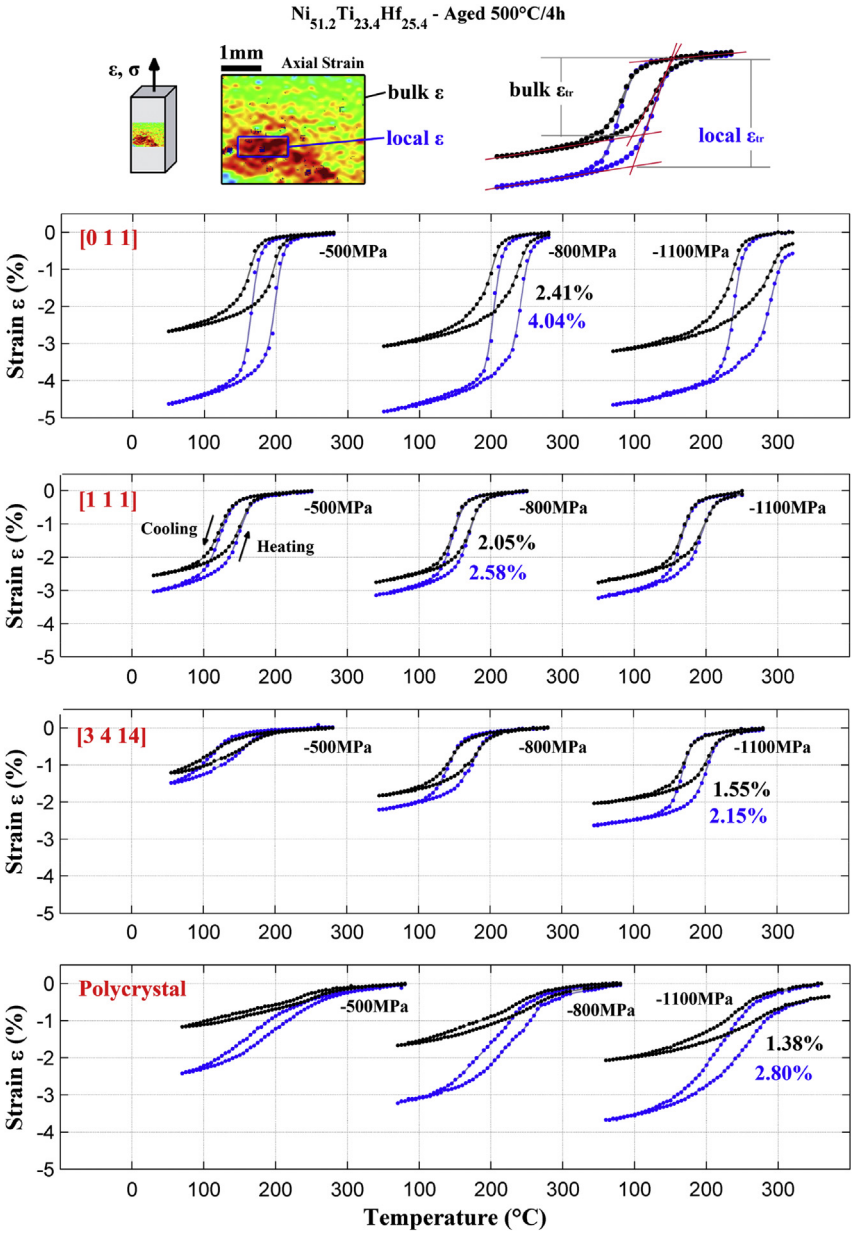

Fig. 3. Influence of the crystal orientation on the isobaric strain-temperature behavior for the $Ni_{51.2}Ti_{23.4}Hf_{25.4}$ alloy aged at 500°C/4 h. The black dots indicate the strain measurements obtained averaging the axial strains over the specimen width (3.6 mm × 2.7 mm, bulk ε), while with blue color are indicated the local strain measurements (local ε). The maximum bulk and local transformation strains are reported for each crystal orientation and for the polycrystal (For interpretation of the references to colour in this figure legend, the reader is referred to the web version of this article).

linear regression using the points in the fully austenite and fully martensite regions, so respectively at temperatures > A_F and <M_F. A third line was obtained using the data in the region of transformation, so approximately in between A_S and A_F. The intersection between the two lines and the third one gives the transformation strain. The procedure was adopted for both the bulk and local strains. The transformation strains were calculated for the strain-temperature curves that show saturation of the transformation strains. For example, for the [1 1 1] orientation, the transformation strain calculated for the curve at −800 MPa and −1100 MPa were the same as all the possible martensite variants were already activated at −800 MPa. Further loading at −1100 MPa leads to irrecoverable strains which are detrimental for the correct measurement of the transformation strains. This is particularly noticeable for the [0 1 1] orientation comparing the strain-temperature curves for the −800 MPa and −1100 MPa stresses. The largest transformation strains were measured for the [0 1 1] orientated single crystal as $\varepsilon^{bulk}_{[0\,1\,1]} = 2.41\%$ bulk strain, and $\varepsilon^{local}_{[0\,1\,1]} = 4.04\%$ local strain. Lower transformation strains were measured for the other two crystal orientations: for the [1 1 1] orientation $\varepsilon^{bulk}_{[1\,1\,1]} = 2.05\%$ and $\varepsilon^{local}_{[1\,1\,1]} = 2.58\%$, for the [3 4 14] orientation $\varepsilon^{bulk}_{[3\,4\,14]} = 1.55\%$ and $\varepsilon^{local}_{[3\,4\,14]} = 2.15\%$. In Fig. 3 is also reported the isobaric behavior of the polycrystal specimen. In this case the transformation strain for the bulk material is relatively low, $\varepsilon^{bulk}_{poly} = 1.38\%$, while locally the transformation strains were measured to be $\varepsilon^{local}_{poly} = 2.80\%$.

Nevertheless the single crystal form of the specimen, non-homogeneous deformations are observed on the DIC strain fields which indicate the heterogeneity of the austenite–to–martensite phase transformation. Fig. 4a shows the DIC strain fields measured for the [0 1 1] orientation for the isobaric experiment conducted at a

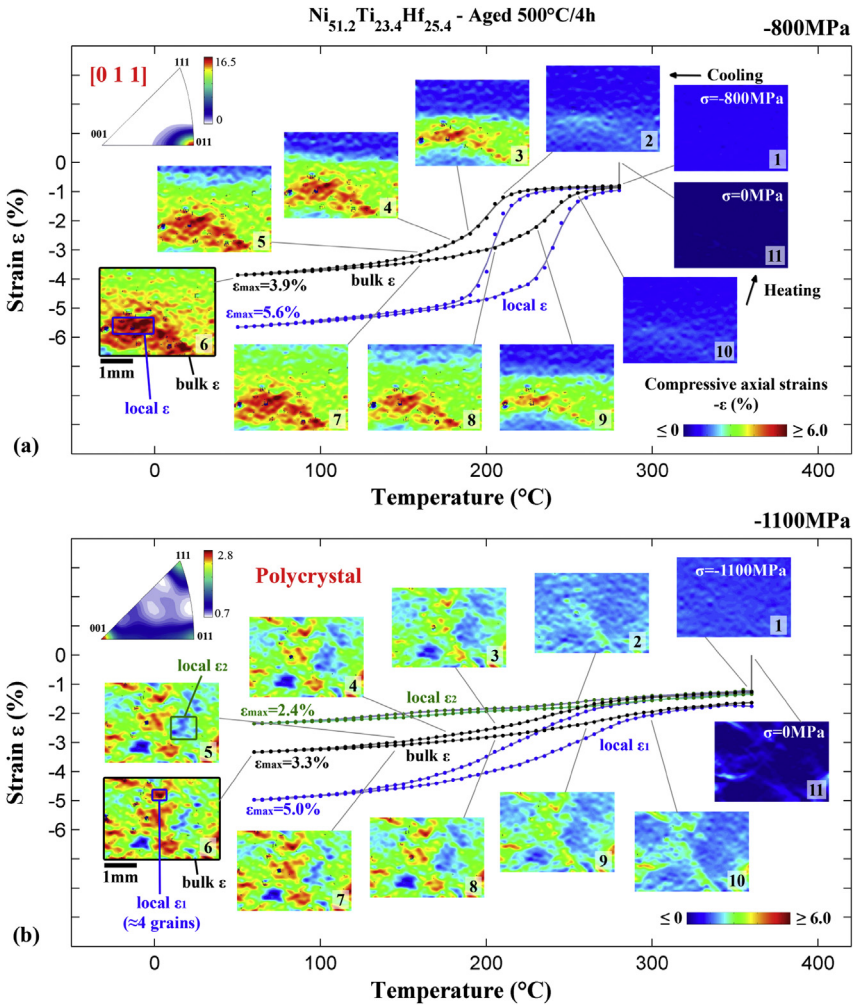

Fig. 4. (a) DIC strain fields for the isobaric experiment along the [011] orientation at −800 MPa. At the lowest experimental temperature (50 °C) the strains are non homogeneous indicating the hetergogeneity of the phase transformation. (b) Temperature-strain behavior for the polycrystal case at −1100 MPa. The bulk strain is compared with a region where high local strains were measured (local ε_1), and with a region where low local strains were measured (local ε_2).

constant stress of −800 MPa. In the stereographic triangle reported in the top-left of Fig. 4a we show the inverse pole figure obtained by means of X-ray diffraction at 300 °C. Along the strain-temperature data we reported the most interesting strain fields measured using DIC. The inset marked 1 shows the strain field after isothermal loading at 280 °C from 0Mpa to −800 MPa. The average compressive axial strain is 0.8%, no strain localizations are observed indicating that at 280 °C the yield stress is higher than 800 MPa. During cooling (from strain field 1 to strain field 6), at the temperature of 210 °C, the local strains (blue curve) diverge from the averaged strains (black curve) indicating the initiation of local phase transformation. From strain field 2 (210 °C) to strain field 6 (50 °C), the phase transformation develops mainly in the central part of the DIC area. The local region showing the largest strain localization was used to calculate the local strain-temperature curve. From strain field 6 to strain field 11, no residual strains remain on the DIC region indicating the complete reversible austenite–martensite phase transformation. The same experimental procedure was adopted for the polycrystal specimen loaded at a constant compressive stress of −1100 MPa (Fig. 4b). The comparison between the [011] crystal with the polycrystal was reported at different stress levels since we aim to compare the local strain fields at the stress level showing the maximum transformation strains, avoiding the occurrence of irreversibility. According to the pole figure reported in the top-left of Fig. 4b, the polycrystal specimen shows a random orientation distribution of the grains along the load direction of the specimen, with a small preference for the [011], [001] and [111] orientations. Three temperature-strain curves were reported for the case of the polycrystal specimen.

The localized strain-temperature curve marked with blue color refers to the region marked in the inset 6 (local ε_1). This region of the polycrystal indicates that the average local strains refer to a group of approximately 4 grains (the average grain size is approximately 200 μm). As the polycrystal shows a preference for one of the three [001], [011], [111] grain orientations, this group of grains reasonably possesses a local preferential [011] texture evidenced by the large strain localization. As also indicated in Fig. 3, the transformation strain displayed by this region is 2.80%, which is lower than the maximum (local) measured for the [011] single crystal (4.04%), but higher than the bulk transformation strain of the [011] crystal (2.41%). This suggests that with the adopted DIC image resolution we cannot capture the strain heterogeneity at sub-grain level for the polycrystal specimen. The local transformation strains calculated for the polycrystal specimen (2.80%, blue curve in Fig. 4b) represent the average transformation strains over approximately 4 grains which agrees with the bulk [011] single crystal

transformation strain reported in Fig. 4a as 2.41%. In Fig. 4b we also provide an additional temperature-strain curve in green color calculated averaging the local axial strains for a group of grains (local ε_2) showing negligible transformation strains. The temperature-strain curve clearly indicates that this group of grains does not undergo phase transformation. This can be explained by two different observations. As previously reported, the austenite–to–martensite phase transformation (at zero stress) is not completed as shown in the diffraction pattern in Fig. 2. Nevertheless under stress the nucleation of martensite in energetically favored, this is not sufficient to guarantee that all the grains transform from the austenite phase to the martensite one. This observation is also supported by the DIC strain fields reported for the [011] single crystal (Fig. 4a) which clearly show that not all the single crystal specimen undergoes to a uniform austenite–to–martensite phase transformation. A second factor can be the simultaneous occurrence of a group of grain orientations having low transformation strains (the inverse pole figure shows local [001] texture) along with low local stresses rising from elastic and plastic grain orientation anisotropy.

3.4. Isothermal behavior

In order to investigate the isothermal mechanical behavior of the $Ni_{51.2}Ti_{23.4}Hf_{25.4}$ alloy the [0 1 1] orientation was selected as the orientation showing the largest transformation strains (Fig. 3). Two different aging treatments were selected: the 500°C/4 h optimizes the pseudoelastic behavior for similar compositions [47], the 550°C/10 h maximizes the temperature showing pseudoelasticity. Higher aging temperatures already have already shown to be detrimental for the pseudoelasticity [47].

Perfect shape memory behavior was observed for temperatures lower than 170 °C for the 500°C/4 h aging (Fig. 5). Pseudoelasticity was observed at temperatures higher than 180 °C. In particular, following the 500°C/4 h aging, since the austenite finish temperature is A_F = 220 °C, and the martensite start temperature is M_S = 160 °C, it is important to heat the specimen at T > A_F in order to complete the transformation in austenite and successively slowly cool the specimen at the desired experimental temperature. As expected from DSC results (Fig. 1a), the 550°C/10 h aging provides higher transformation temperatures, in particular pseudoelasticity was found starting from 240 °C (Fig. 5).

The stress–strain behavior was further investigated using local strain measurements. Fig. 6a and b shows the optimum pseudoelastic stress–strain curves for the selected aging treatments for the [0 1 1] crystal orientation. Comparing the stress–strain responses for the two agings, it is evident how the 550°C/10 h aging deteriorates the pseudoelastic behavior. The stress hysteresis for the 500°C/4 h aged specimen is much lower than the hysteresis for the 550°C/10 h aged specimen. Moreover, for the 550°C/10 h aged specimen, irrecoverable plastic strain remains upon unloading. For the 500°C/4 h aging, the temperature showing the optimum pseudoelastic behavior was found to be 200 °C (Fig. 6a), which is below the A_F temperature (220 °C). DIC strain fields enable to capture the nucleation of phase transformation throught the local strain measurements (blue line) for a region of the specimen were high local strains were measured (see blue box in inset marked 5). As observed during the isobaric experiments, the phase transformation is heterogeneous and the transformation strains determined fo the averaged axial strains and for the local axial strains are strongly affected. The transformation strain measured for the averaged axial strain was 2.45%, while locally is 3.86%. This reveal the importance of DIC strain measurement in order to properly estimate the maximum transformation strains. Similiarly, for the 550°C/10 h aging (Fig. 6b), DIC strain measurements provide interesting characteristics on the heterogeneous deformation. While the average axial strain measurements provide almost the same transformation strain (2.43%), the local strain mesaurements indicate that for the 550°C/10 h aging the maximum transformation strains are lower (3.19% versus 3.86%).

3.5. Thermodynamics

Calculation of the entropy for shape memory alloys reveals

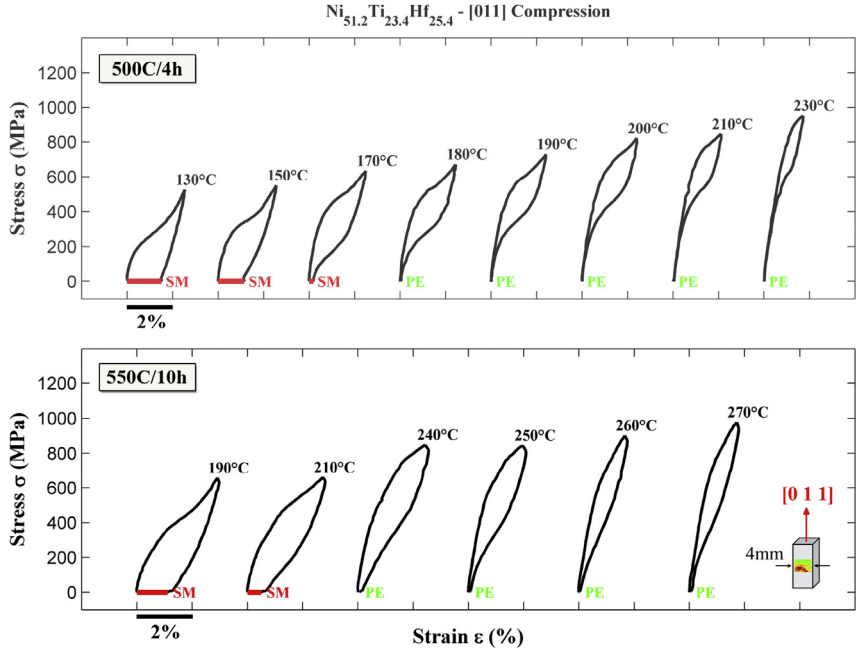

Fig. 5. Comparison between the isothermal stress–strain curves for the [011] orientation for the specimens aged at 500°C/4 h and 550 °C/10 h. The 500 °C/4 h aging determines the best pseudoelastic behavior for the investigated $Ni_{51.2}Ti_{23.4}Hf_{25.4}$ alloy.

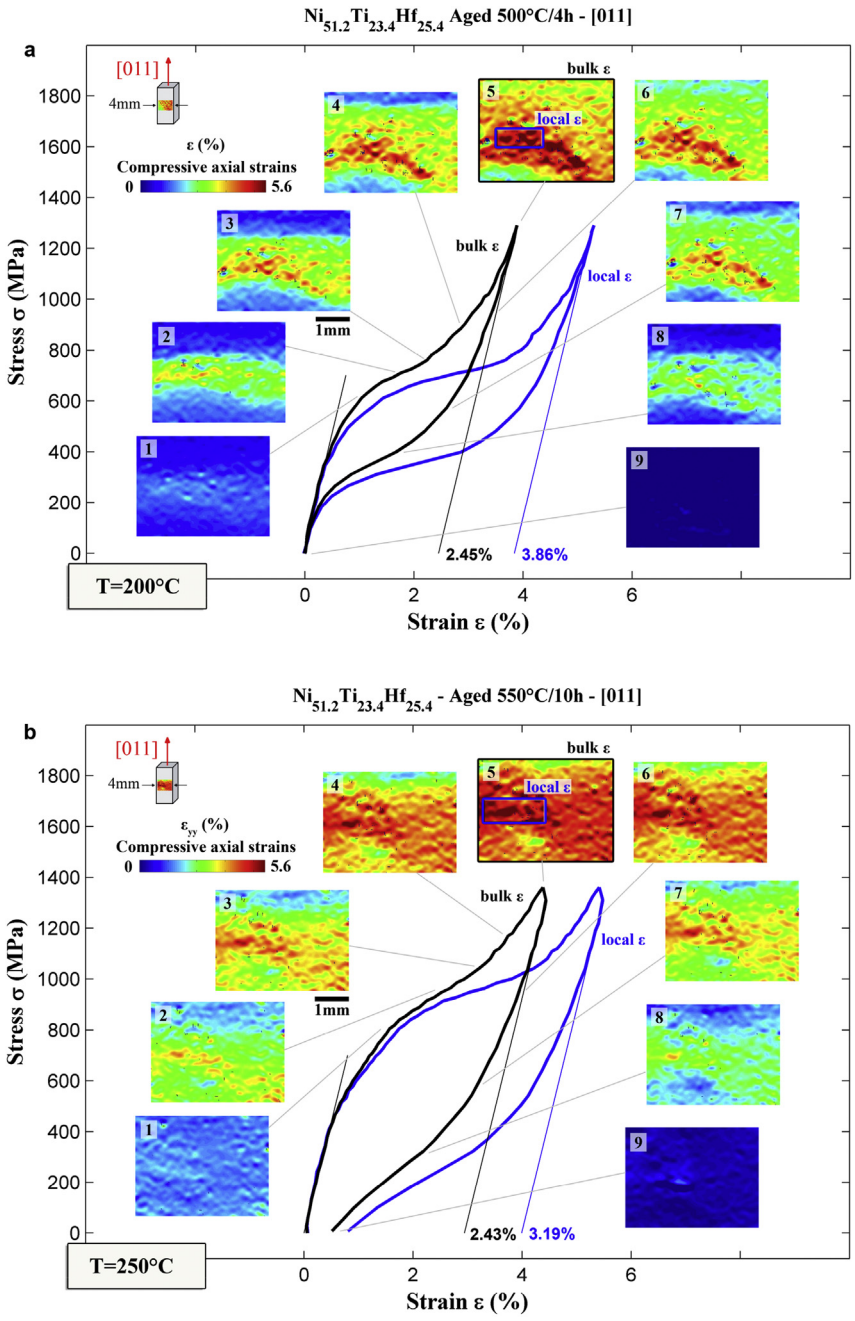

Fig. 6. (a) Isothermal stress–strain curves for the [011] orientation for the specimen aged at 500°C/4 h and tested at 200 °C in fully austenite. (b). Isothermal stress–strain curves for the [011] orientation for the specimen aged at 550 °C/10 h and tested at 250 °C in fully austenite.

interesting aspects of the thermodynamics of the phase transformation associated with transformation strains and transformation temperatures. The Clausius–Clapeyron (CC) equation is written as follow

$$\frac{d\sigma^T}{dT} = \frac{-\Delta s}{\varepsilon^T} = \frac{-\Delta h\rho}{T\varepsilon^T} \tag{1}$$

The term $d\sigma^T/dT$ indicates the CC slope of the temperature-critical stress in the martensite-stress induced temperature range (the slope indicated in Fig. 7), ε^T is the transformation strain (which is orientation dependent), the variation of enthalpy Δh from austenite to martensite phases is determined from the DSC curves reported in Fig. 1a. The equilibrium temperature $T = T_0 = 1/2(M_S + A_F)$ is chosen according the Tong and Wayman proposal [50]. Fig. 7 summarizes the orientation-dependence of the critical stress with temperature. Equation (1) indicates that the CC slope depends on the crystal orientation. In Fig. 7 is shown the critical stress dependence on the temperature calculated from the isothermal stress–strain curves (Fig. 4) for the [1 1 1] and [0 1 1] orientations. For the [1 1 1] orientation we measured an average CC slope of 10.3 MPa/°C, while for the [0 1 1] orientation we measured 7.2 MPa/°C. The aging does not affect the CC slope, while it influences the equilibrium temperature T_0 (see equation (1)). The change in enthalpy Δh is not influenced by the crystal orientation (Table 1), while it depends on the aging treatment adopted. The transformation strains predicted using the CC equations agrees

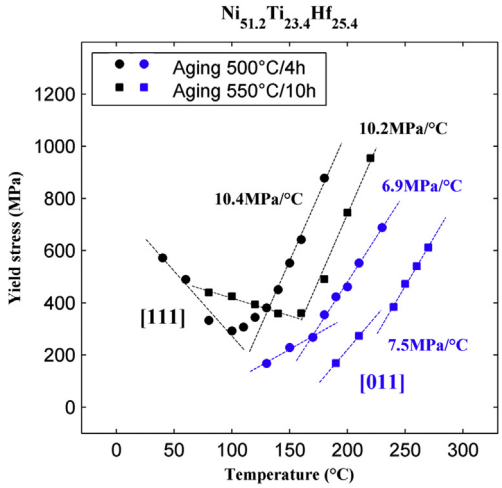

Fig. 7. Yield stress function of temperature for the 500 °C/4 h and the 550 °C/10 h aging treatments for the [111] and [011] crystal orientations.

with the experimental ones obtained during isobaric experiments (Table 1 and Fig. 3).

3.6. Theoretical transformation strains

The maximum transformation strains determined from isobaric strain-temperature experiments are reported in the stereographic triangle in Fig. 8. The theoretical transformation strains were calculated via lattice deformation theory (LDT) for the cubic B2 to orthorhombic B19 lattices transformation. LDT considers the fully transformation from the austenite crystal to the martensite crystal neglecting twinning. A close agreement was found for the [0 1 1] and [3 4 14] orientations, while the transformation strains for the [1 1 1] orientation are lower than the strains predicted with LTD. Nevertheless for the [1 1 1] orientation the strains are lower than predicted, we notice the trend is well predicted.

4. Discussion

One of the most intriguing questions regarding NiTiHf shape memory studies is the difference between the theoretical predicted transformation strains with the strains measured experimentally for the polycrystal and, in particular, for single crystals [15,24,25,27,28,51]. In order to address this question, in the present work, single crystals and polycrystals of the new $Ni_{51.2}Ti_{23.4}Hf_{25.4}$ alloy were studied using DIC technique. We combined strain measurements via DIC and microstructural characterization via X-ray diffraction in order to provide a straightforward comparison between the experimental strains and the strains predicted by LDT. We focused on the orientation dependence of NiTiHf alloys for high(Hf) content (>25 at %), where the cubic austenite to orthorhombic martensite phase transformation occurs.

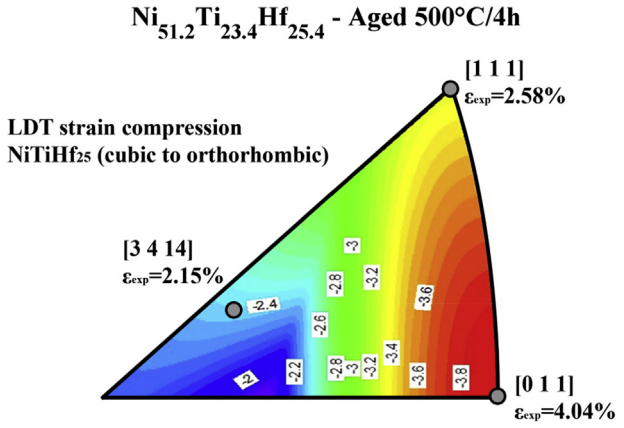

Fig. 8. Maximum transformation strains obtained from isobaric experiments using local DIC strain measurements. The results are compared with the maximum theoretical transformation strains calculated using LDT.

4.1. Single crystal transformation strains

The transformation strains were determined from the isobaric experiments to be $\varepsilon^{local}_{[0\,1\,1]} = 4.04\%$, $\varepsilon^{local}_{[1\,1\,1]} = 2.58\%$ and $\varepsilon^{local}_{[3\,4\,14]} = 2.15\%$ (Fig. 3). These values have shown to be consistent with the theoretical transformation strains determined with LDT according the phase transformation from the cubic austenite B2 to the orthorhombic martensite B19 (Fig. 8). Nevertheless the single crystal form of the specimens, DIC strain fields (isobaric experiment in Fig. 4, and isothermal experiments in Fig. 6a and b) shows that the austenite–martensite phase transformation front does not propagate homogeneously over the DIC region. For example, in Fig. 6a the pseudoelastic behavior of the specimen shows an average transformation strain of 2.45%, while locally we measured transformation strains up to 3.86%. According to the Xray diffraction data (Fig. 2), peaks from B2 austenite are still present at RT nevertheless the martensite finish temperature is 110 °C for the 600°C/4 h aging treatment. XRD results and DIC strain measurements suggest that some locations of the specimens are less favorable to martensitic transformation even under an applied stress (Fig. 6a and b). The ideal crystal transformation from austenite phase to the martensite phase is then not completely realized leading to the underestimation of the transformation strains using classical strain measurement techniques, e.g. extensometers.

4.2. Single crystal versus polycrystal transformation strains

In order to compare the transformation strains for the polycrystal and the single crystals, it is necessary to elucidate the meaning of bulk strains and local strains measured with DIC. As previously discussed, the transformation strains obtained averaging the axial strains over the DIC region for the single crystals (approximately 3 mm × 4 mm) represent the average behavior for the selected orientation (bulk strain). Such measurement technique

Table 1
Transformation strains estimated from the Clausius–Clapeyron equation for the $Ni_{51.2}Ti_{23.4}Hf_{25.4}$ [011] and [111] orientations studied in this work.

Aging	Orientation	Entalphy$_{A\rightarrow M}$ [J/g]	$T_0 = 1/2(M_S + A_F)$ (K)	$(d\sigma^T/dT)_{exp}$ (MPa/K)	$(\varepsilon_{transf})_{exp}$ (%)	$(\varepsilon_{transf})_{C-C}$ (%)
500°C/4 h	[011]	12.786	466.15	6.9	4.04	3.72
550°C/10 h		17.087	582.15	7.5	3.92	3.66
500°C/4 h	[111]	12.786	466.15	10.4	2.58	2.47
550°C/10 h		17.087	582.15	10.2	2.55	2.69

considers both the transformed and untransformed regions of the specimen and it underestimates the effective transformation strain. Using local strain measurements, we provided the correct estimation of the transformation strains considering only the specimen region that completely undergoes the austenite–martensite phase transformation (approximately a region of 1 mm × 0.75 mm).

The polycrystal is formed by an aggregate of different grains having the orientation distribution as represented in the inverse pole figure of Fig. 4b. Moreover, the average grain size is 200 μm. From the inverse pole figure of the polycrystal is evident that the orientation distribution of the polycrystal contains multiple grain orientations, including those close to the (011) pole. According to the theoretical calculations (Fig. 8), the grains with an orientation close to (011) show the largest transformation strain. The strain maps provided for the polycrystal experiment (Fig. 4b) show regions of the specimen with high local transformation strains (the maximum measured as 2.80%). These local transformation strains are averaged over a region of the specimen that contains approximately 4 grains. It is reasonable to assume that the largest local transformation strains measured in the polycrystal correspond to group of grains oriented along the 011 pole. Moreover, the local transformation strains measured for the polycrystal case (2.80%) are in agreement with the results obtained for the [011] crystal orientation bulk strains (2.41%). In this comparison, the local transformation strains measured for the polycrystal cannot reach the local transformation strains of the [011] orientation only because of a limitation on the DIC resolution which, with the adopted experimental set-up, cannot capture sub-grain strain heterogeneities.

It is also interesting to note that the bulk transformation strain for the polycrystal case (1.38%) is lower compared to any of the bulk single crystal transformation strains. DIC strain fields show that different regions of the polycrystal specimen do not undergo phase transformation during the cooling/heating thermal cycle (Fig. 4). Un-complete austenite–martensite phase transformation was then observed also in the polycrystal specimen; this explains the low bulk transformation strains measured for the polycrystal. This observation is of fundamental importance in explaining the discrepancy between the experimental transformation strains measured with classical techniques and the ones calculated theoretically. Besides, in the polycrystal case, the incomplete austenite–martensite transformation is also made difficult due to the presence of the grain boundaries and a non homogeneous precipitate distribution which can further inhibit the volume fraction of the transformed phase.

4.3. Transformation temperatures

Compared to similar NiTiHf alloys, the present $Ni_{51.2}Ti_{23.4}Hf_{25.4}$ composition shows very high transformation temperatures. As a comparison, the $Ni_{50.3}Ti_{29.7}Hf_{20}$ composition shows $A_F = 210$ °C for the specimen aged 600°C/3 h [5], while the present composition shows $A_F = 380$ °C for the homogenized specimen, and $A_F = 300$ °C for the specimen aged 600°C/4 h. The drawback of utilizing these heat treatments for further TTs increments is the decrease of the shape memory and pseudoelastic properties. Larger precipitate size and inter-particle distances are obtained with high aging temperatures (>550 °C), and long aging times (>4 h). The change in precipitate geometry and distribution lowers the strength of the matrix favoring the irrecoverable plastic deformations. In the present work, we optimized the TTs and the shape memory and pseudoelastic behavior of the $Ni_{51.2}Ti_{23.4}Hf_{25.4}$ by an aging 500°C/4 h. This aging results in a perfect pseudoelastic behavior at temperatures higher than 200 °C. We also show that with the 550°C/10 h aging the pseudoelastic behavior was found at temperatures higher than 250 °C with a decrease of the transformation strain, 3.19% versus 3.86%. The transformation strain values reported and compared in Fig. 8 were calculated for the samples aged at 500°C/4 h. As reported by several authors for similar compositions, fine precipitates are observed for this aging treatment [5]. As the measured local transformation strains are close to the theoretical ones, we conclude that the precipitates do not provide a strong barrier to the austenite–martensite phase transformation.

4.4. Pseudoelasticity

Pseudoelasticity was found at temperatures higher than T_{SE}>180 °C for the [011] orientation aged at 500°C/4 h, and T_{SE}>250 °C for the 550°C/10 h aging treatment. Short aging times provide fine and coherent precipitates which strengthen the matrix and allow the martensite to develop resulting in a non-obstructed martensite growth. On the other side, longer aging treatments are detrimental for the transformation strains as the increment of the precipitate size and loss of coherency obstacle to the growth of the martensite. This results in a reduction of the transformation strains. Since longer aging treatments enable to deplete Ni from the matrix, it is possible to further increase the TTs with even longer aging times resulting, on the other side, on the loss of precipitate coherency with the B2 austenite. The resulted loss of pseudoelasticity can be seen comparing the stress–strain curves in Fig. 6a (500 °C/4 h) and Fig. 6b (550 °C/10 h).

4.5. Thermodynamics

Enthalpy variations were derived from DSC curves and the Clausius–Clapeyron equation (1) was used to verify the transformation strains. A close agreement was found for the [011] and [111] orientations (Table 1). The slopes of the yield stress-temperature curves in the pseudoelastic window found for the [111] and [011] orientations, 10.3 and 7.3 MPa/°C respectively, are consistent with the results already published previously for similar NiTi and NiTiHf alloys. For the aging treatments adopted in this study (500°C/4 h versus 550°C/10 h), negligible influence on the CC slope was found.

5. Conclusions

In this work we present the functional behavior of the new $Ni_{51.2}Ti_{23.4}Hf_{25.4}$ alloy for three crystal orientation [0 1 1], [1 1 1] and [3 4 14], along with a comparison with the polycrystal behavior. The work supports the following conclusions:

- The transformation strains determined from isobaric experiments for the three single crystal orientations are $\varepsilon^{local}_{[0\ 1\ 1]} = 4.04\%$, $\varepsilon^{local}_{[1\ 1\ 1]} = 2.58\%$ and $\varepsilon^{local}_{[3\ 4\ 14]} = 2.15\%$. These values are in agreement with the theoretical values estimated using LDT calculations based on the B2 cubic austenite to the B19 orthorhombic martensite phase transformation.
- X-ray diffraction performed on aged specimen shows peaks from the orthorhombic phase and from the cubic phase in martensite state confirming the incomplete austenite–to–martensite phase transformation; non uniform phase transformation was also found in the single crystal specimens during isothermal and isobaric experiments; this was revealed by large strain heterogeneities measured using the DIC technique.
- The bulk transformation strain for the polycrystal specimen is lower than any of the single crystal orientations tested in this work. On the other side, local strain measurements show that high local transformation strains arise for well-favored local [011] texturized group of grains. In perspective, this suggests

that the [011] texturized polycrystal maximizes the transformation strains.
- The new $Ni_{51.2}Ti_{23.4}Hf_{25.4}$ alloy shows high TTs (>250 °C) along with high strength (>1000 MPa) making it suitable for high temperature actuator applications.

Acknowledgments

The work was supported by NSF-CMMI 1333884 which is gratefully acknowledged. X-ray diffraction was carried out in the Frederick Seitz Materials Research Laboratory Central Facilities, University of Illinois; the authors acknowledge Dr. Mauro Sardela for assistance with it. Prof. Chumlyakov acknowledges the RSF project 14-29-00012. The authors are also thankful to Mr. George Li for the lattice deformation theory based transformation strain calculations.

References

[1] D.N. AbuJudon, P.E. Thoma, M.-Y. Kao, D.R. Angst, High. Transform. Temp. shape Mem. alloy 5 (114) (1992) 504.
[2] R.D. Angst, E.P. Thoma, Y.M. Kao, The Effect of Hafnium Content on the Transformation Temperatures of Ni[49]Ti[51-x]Hf[x] Shape Memory Alloys, EDP sciences, Les Ulis, FRANCE, 1995.
[3] G.S. Firstov, J. Van Humbeeck, Y.N. Koval, High-temperature shape memory alloys: Some recent developments, Mater. Sci. Eng. A 378 (2004) 2.
[4] J. Ma, I. Karaman, R.D. Noebe, High temperature shape memory alloys, Int. Mater. Rev. 55 (2010) 257.
[5] H.E. Karaca, E. Acar, H. Tobe, S.M. Saghaian, NiTiHf-based shape memory alloys, Mater. Sci. Technol. 30 (2014) 1530.
[6] S-h Kang, T-h Nam, Crystal structure of (TiHf)Ni phase formed in a 20Ti–50Ni–30Hf (at.%) alloy, Met. Mater. Int. 7 (2001) 443.
[7] S. Sanjabi, Y.Z. Cao, Z.H. Barber, Multi-target sputter deposition of Ni50Ti50-xHfx shape memory thin films for high temperature microactuator application, Sensors Actuators A Phys. 121 (2005) 543.
[8] Y. Tong, Y. Liu, J. Miao, Phase transformation in NiTiHf shape memory alloy thin films, Thin Solid Films 516 (2008) 5393.
[9] S. Besseghini, E. Villa, A. Tuissi, Ni·Ti·Hf shape memory alloy: effect of aging and thermal cycling, Mater. Sci. Eng. A 273–275 (1999) 390.
[10] O. Benafan, A. Garg, R.D. Noebe, G.S. Bigelow, S.A. Padula Ii, D.J. Gaydosh, N. Schell, J.H. Mabe, R. Vaidyanathan, Mechanical and functional behavior of a Ni-rich Ni50.3Ti 29.7Hf20 high temperature shape memory alloy, Intermetallics 50 (2014) 94.
[11] O. Benafan, R.D. Noebe, S.A. Padula Ii, R. Vaidyanathan, Microstructural response during isothermal and isobaric loading of a precipitation-strengthened Ni-29.7Ti-20Hf high-temperature shape memory alloy, Metallurgical Mater. Trans. A Phys. Metallurgy Mater. Sci. 43 (2012) 4539.
[12] G.S. Bigelow, A. Garg, S.A. Padula Ii, D.J. Gaydosh, R.D. Noebe, Load-biased shape-memory and superelastic properties of a precipitation strengthened high-temperature Ni 50.3Ti 29.7Hf 20 alloy, Scr. Mater. 64 (2011) 725.
[13] D.R. Coughlin, P.J. Phillips, G.S. Bigelow, A. Garg, R.D. Noebe, M.J. Mills, Characterization of the microstructure and mechanical properties of a 50.3Ni–29.7Ti–20Hf shape memory alloy, Scr. Mater. 67 (2012) 112.
[14] C.M. Denowh, D.A. Miller, Thermomechanical training and characterization of NiTiHf and NiTiHfCu high temperature shape memory alloys, Smart Mater. Struct. 21 (2012).
[15] H.E. Karaca, S.M. Saghaian, B. Basaran, G.S. Bigelow, R.D. Noebe, Y.I. Chumlyakov, Compressive response of nickel-rich NiTiHf high-temperature shape memory single crystals along the [1 1 1] orientation, Scr. Mater. 65 (2011) 577.
[16] H.E. Karaca, S.M. Saghaian, G. Ded, H. Tobe, B. Basaran, H.J. Maier, R.D. Noebe, Y.I. Chumlyakov, Effects of nanoprecipitation on the shape memory and material properties of an Ni-rich NiTiHf high temperature shape memory alloy, Acta Mater. 61 (2013) 7422.
[17] W. Cai, X.L. Meng, L.C. Zhao, Recent development of TiNi-based shape memory alloys, Curr. Opin. Solid State Mater. Sci. 9 (2005) 296.
[18] X.L. Meng, W. Cai, Y.D. Fu, Q.F. Li, J.X. Zhang, L.C. Zhao, Shape-memory behaviors in an aged Ni-rich TiNiHf high temperature shape-memory alloy, Intermetallics 16 (2008) 698.
[19] X.L. Meng, W. Cai, Y.F. Zheng, L.C. Zhao, Phase transformation and precipitation in aged Ti-Ni-Hf high-temperature shape memory alloys, Mater. Sci. Eng. A 438–440 (2006) 666.
[20] R. Santamarta, R. Arróyave, J. Pons, A. Evirgen, I. Karaman, H.E. Karaca, R.D. Noebe, TEM study of structural and microstructural characteristics of a precipitate phase in Ni-rich Ni–Ti–Hf and Ni–Ti–Zr shape memory alloys, Acta Mater. 61 (2013) 6191.
[21] K. Bhattacharya, Microstructure of Martensite: Why it Forms and How it Gives Rise to the Shape-memory Effect, Oxford University Press, Oxford, New York, 2003.
[22] O. Matsumoto, S. Miyazaki, K. Otsuka, H. Tamura, Crystallography of martensitic transformation in Ti·Ni single crystals, Acta Metall. 35 (1987) 2137.
[23] S. Miyazaki, S. Kimura, K. Otsuka, Y. Suzuki, The habit plane and transformation strains associated with the martensitic transformation in Ti-Ni single crystals, Scr. Metall. 18 (1984) 883.
[24] H.E. Karaca, E. Acar, B. Basaran, R.D. Noebe, G. Bigelow, A. Garg, F. Yang, M.J. Mills, Y.I. Chumlyakov, Effects of aging on [111] oriented NiTiHfPd single crystals under compression, Scr. Mater. 67 (2012) 728.
[25] H.E. Karaca, E. Acar, B. Basaran, R.D. Noebe, Y.I. Chumlyakov, Superelastic response and damping capacity of ultrahigh-strength [111]-oriented NiTiHfPd single crystals, Scr. Mater. 67 (2012) 447.
[26] E. Acar, H.E. Karaca, B. Basaran, F. Yang, M.J. Mills, R.D. Noebe, Y.I. Chumlyakov, Role of aging time on the microstructure and shape memory properties of NiTiHfPd single crystals, Mater. Sci. Eng. A 573 (2013) 161.
[27] A.P. Stebner, G.S. Bigelow, J. Yang, D.P. Shukla, S.M. Saghaian, R. Rogers, A. Garg, H.E. Karaca, Y. Chumlyakov, K. Bhattacharya, R.D. Noebe, Transformation strains and temperatures of a nickel–titanium–hafnium high temperature shape memory alloy, Acta Mater. 76 (2014) 40.
[28] S.M. Saghaian, H.E. Karaca, H. Tobe, M. Souri, R. Noebe, Y.I. Chumlyakov, Effects of aging on the shape memory behavior of Ni-rich Ni50.3Ti29.7Hf20 single crystals, Acta Mater. 87 (2015) 128.
[29] X.D. Han, W.H. Zou, R. Wang, Z. Zhang, D.Z. Yang, Structure and substructure of martensite in a Ti36.5Ni48.5Hf15 high temperature shape memory alloy, Acta Mater. 44 (1996) 3711.
[30] X.D. Han, R. Wang, Z. Zhang, D.Z. Yang, In situ observations of the reverse martensitic transformations in a TiNiHf high temperature shape memory alloy, Mater. Lett. 30 (1997) 23.
[31] Y.F. Zheng, W. Cai, J.X. Zhang, Y.Q. Wang, L.C. Zhao, H.Q. Ye, High-resolution electron microscopy study on the substructure of Ti-Ni-Hf B19′ Martensite, Mater. Lett. 36 (1998) 142.
[32] Y.F. Zheng, L.C. Zhao, H.Q. Ye, HREM study on the intervariant structure of Ti-Ni-Hf B19′ martensite, Scr. Mater. 38 (1998) 1249.
[33] X.L. Meng, Y.F. Zheng, Z. Wang, L.C. Zhao, Effect of aging on the phase transformation and mechanical behavior of Ti36Ni49Hf15 high temperature shape memory alloy, Scr. Mater. 42 (2000) 341.
[34] T. Chang-Long, C. Wei, T. Xiao-Hua, First-principles study on the effect of Hf content on martensitic transformation temperature of TiNiHf alloy, Chin. Phys. 15 (2006) 2718.
[35] K.S. Suresh, D.I. Kim, S.K. Bhaumik, S. Suwas, Evolution and stability of phases in a high temperature shape memory alloy Ni49.4Ti38.6Hf12, Intermetallics 44 (2014) 18.
[36] K.S. Suresh, D.I. Kim, S.K. Bhaumik, S. Suwas, Evolution of microstructure and texture in Ni49.4Ti38.6Hf12 shape memory alloy during hot rolling, Intermetallics 42 (2013) 1.
[37] J.-W. Jo, N.-S. Kim, K.-H. Kim, J.-T. Yeom, J.-I. Kim, T.-H. Nam, Effect of Ni Content on the Aging Behavior of Ti-xNi-12Hf (x = 50.2~51.0)(at%) Alloys, J. Appl. Statistics 6 (2014) 2015.
[38] X.L. Meng, Y.D. Fu, W. Cai, J.X. Zhang, Q.F. Li, L.C. Zhao, in: Martensitic Transformation Behavior and Shape Memory Effect of an Aged Ni-rich Ti-ni-hf High Temperature Shape Memory Alloy, 138, 2008, p. 399.
[39] A. Evirgen, F. Basner, I. Karaman, R.D. Noebe, J. Pons, R. Santamarta, Effect of aging on the martensitic transformation characteristics of a Ni-rich NiTiHf high temperature shape memory alloy, Funct. Mater. Lett. 05 (2012) 1250038.
[40] D.R. Coughlin, Characterization of Stoichiometric and Aging Effects on NiTiHf High Temperature Shape Memory Alloys, The Ohio State University, 2013.
[41] K. Gall, H. Sehitoglu, Y.I. Chumlyakov, I.V. Kireeva, H.J. Maier, The Influence of Aging on Critical Transformation Stress Levels and Martensite Start Temperatures in NiTi: Part II—Discussion of Experimental Results, J. Eng. Mater. Technol. 121 (1999) 28.
[42] K. Gall, H. Sehitoglu, Y.I. Chumlyakov, I.V. Kireeva, H.J. Maier, The Influence of Aging on Critical Transformation Stress Levels and Martensite Start Temperatures in NiTi: Part I—Aged Microstructure and Micro-Mechanical Modeling, J. Eng. Mater. Technol. 121 (1999) 19.
[43] F. Yang, D.R. Coughlin, P.J. Phillips, L. Yang, A. Devaraj, L. Kovarik, R.D. Noebe, M.J. Mills, Structure analysis of a precipitate phase in an Ni-rich high-temperature NiTiHf shape memory alloy, Acta Mater. 61 (2013) 3335.
[44] M.A. Sutton, J.-J. Orteu, H. Schreier, Image Correlation for Shape, Motion and Deformation Measurements: Basic Concepts, Theory and Applications, 2009.
[45] C. Efstathiou, H. Sehitoglu, J. Carroll, J. Lambros, H.J. Maier, Full-field strain evolution during intermartensitic transformations in single-crystal NiFeGa, Acta Mater. 56 (2008) 3791.
[46] R.F. Hamilton, S. Dilibal, H. Sehitoglu, H.J. Maier, Underlying mechanism of dual hysteresis in NiMnGa single crystals, Mater. Sci. Eng. A 2011 (1877) 528.
[47] L. Patriarca, H. Sehitoglu, High-temperature superelasticity of Ni50.6Ti24.4Hf25.0 shape memory alloy, Scr. Mater. 101 (2015) 12.
[48] R.F. Hamilton, H. Sehitoglu, Y. Chumlyakov, H.J. Maier, Stress dependence of the hysteresis in single crystal NiTi alloys, Acta Mater. 52 (2004) 3383.
[49] J. Wang, H. Sehitoglu, Modelling of martensite slip and twinning in NiTiHf shape memory alloys, Philos. Mag. 94 (2014) 2297.
[50] H.C. Tong, C.M. Wayman, Characteristic temperatures and other properties of thermoelastic martensites, Acta Metall. 22 (1974) 887.
[51] E. Acar, H.E. Karaca, H. Tobe, R.D. Noebe, Y.I. Chumlyakov, Orientation dependence of the shape memory properties in aged Ni45.3Ti29.7Hf20Pd5 single crystals, Intermetallics 54 (2014) 60.